Bottlebrush Elastomers: A New Platform for Freestanding Electroactuation

Mohammad Vatankhah-Varnoosfaderani, William F. M. Daniel, Alexandr P. Zhushma, Qiaoxi Li, Benjamin J. Morgan, Krzysztof Matyjaszewski, Daniel P. Armstrong, Richard J. Spontak, Andrey V. Dobrynin, and Sergei S. Sheiko**

Dielectric elastomers (DEs) are the leading technology for artificial muscles due to a favorable combination of large stroke, fast response, and high energy density.[1–5] However, at large actuations, DEs are prone to spontaneous rupture from electromechanical instability. This shortcoming is currently circumvented by chemical or physical bracing,[6–8] which increases the bulk of the total actuator assembly leading to significant cutbacks in device efficiency and utility.[9,10] Now, we present a molecular design platform for the creation of freestanding actuators that allow for large stroke (>300%) at low applied fields (<10 V μm^{-1}) in unconstrained as-cast shapes. This approach is based on the bottlebrush architecture, which features inherently strained polymer networks that eliminate electromechanical instability and the need for bracing. Through accurate and independent control of the degree of polymerization (DP) of the side-chains (n_{sc}), the DP of the spacer between neighboring sidechains (n_g), and the DP of the backbone of bottlebrush network strands (n_x), we obtain effective actuation properties on par with commercial actuators with the advantage of lighter weight, lower voltage operation, and ease of fabrication, which open new opportunities in soft-matter robotics.[11–13]

The pursuit of high-performance artificial muscles has been bolstered by the introduction of DEs that readily undergo sizable (>100%), rapid (>1 kHz), and reversible deformations in response to an electric field.[1,14–19] These unique attributes, however, are impeded by premature electrical breakdown,[20] which can be visualized using the simplest actuator configuration, a DE film sandwiched between two compliant electrodes (**Figure 1**a). The transverse contraction $\lambda = h/h_0$ and subsequent areal expansion $\lambda_a = \lambda^{-1}$ are governed by the mechanical properties of the film through a relationship between the applied voltage Φ and the resultant true stress $\sigma_{true}(\lambda)$, given by $\Phi \sim \lambda\sqrt{|\sigma_{true}(\lambda)|}$. For conventional elastomers composed of flexible strands and exhibiting a strain-independent elastic modulus (line 1 in Figure 1b), this relationship displays a maximum in areal expansion at $\lambda_a^{EMI} \cong \lambda^{-1} \cong 1.59$ (line 1 in Figure 1c), which designates the onset of an electromechanical instability (EMI). In voltage-controlled operations, the EMI generates a snap-through compression in the film, which is typically followed by electrical breakdown, as indicated by the dashed arrow in Figure 1c. As discussed previously,[21] prestretching and then bracing a DE with either physical methods (by fastening to a rigid frame[1] or lamination) or chemical methods (by introducing an interpenetrating polymer network[7] or swelling in a solvent followed by mechanical prestrain[22,23]) promotes an increase in modulus during deformation (strain-stiffening), which in turn prevents EMI. It should also be noted that controlling actuation pressure modulation can also avoid EMI.[24] However, the above methods lead to increased device weight and size (rigid frames), decreased DE flexibility (interpenetrating networks), solvent leakage on actuation (swelling), and interfacial failure (lamination). The challenge is therefore to develop a single-component material with inherent and rapid onset of strain-stiffening such that it does not require any type of preactuation manipulation or bracing. Moreover, designing elastomers possessing both low modulus and high extensibility enables large stroke and low-voltage operation required for biomedical applications.[19,25–27] Finally, we desire to tune both stiffness and elasticity over a broad range without altering network chemistry or incorporation of a second component, such as an oligomer, solvent, crosslinker, or nanoscale filler.

Such inherently prestrained, single-component elastomers can be created by introducing multiple, covalently-linked side chains along the network strands, yielding so-called bottlebrush networks composed of extended strands and possessing low Young's moduli (line 3 in Figure 1b). An important consideration in the molecular design of DEs is that the polymer chains in bottlebrush elastomers are disentangled, which releases the molecular constraint on high extensibility. This unique combination of mechanical properties—inherent strain-stiffening, low modulus, and high elasticity—affords controllable electroactuation of thick, freestanding DE samples over a broad range of strains at low voltages. **Figure 2** shows two characteristic

Dr. M. Vatankhah-Varnoosfaderani, W. F. M. Daniel, A. P. Zhushma, Q. Li, B. J. Morgan, Prof. S. S. Sheiko
Department of Chemistry
University of North Carolina
Chapel Hill, NC 27599, USA
E-mail: sergei@email.unc.edu
Prof. K. Matyjaszewski
Department of Chemistry
Carnegie Mellon University
Pittsburgh, PA 15213, USA
D. P. Armstrong, Prof. R. J. Spontak
Department of Chemical and Biomolecular Engineering
Department of Materials Science and Engineering
North Carolina State University
Raleigh, NC 27695, USA
Prof. A. V. Dobrynin
Department of Polymer Science
University of Akron
Akron, OH 44325, USA
E-mail: adobrynin@uakron.edu

DOI: 10.1002/adma.201604209

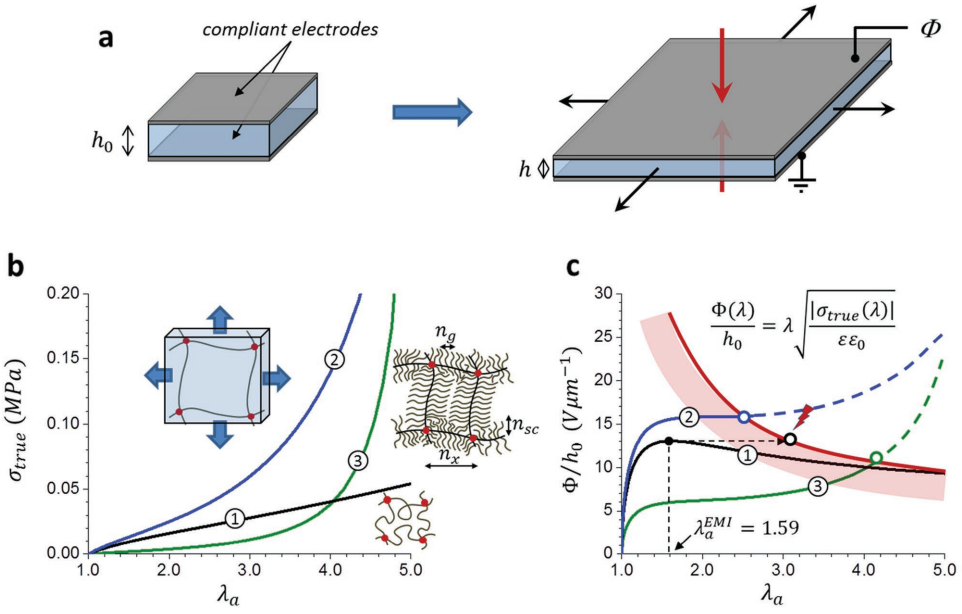

Figure 1. Electroactuation of prestrained elastomers. a) A dielectric elastomer sandwiched between two compliant electrodes undergoes uniaxial compression $\lambda = h/h_0$ and corresponding radial expansion upon application of an external electric field of potential Φ. b) Variation of the true stress as a function of the areal expansion $\lambda_a = \lambda^{-1}$ for three types of polymer networks: ① a conventional elastomer with coiled network strands that exhibit linear elasticity, ② an equibiaxially prestrained conventional elastomer displays distinct strain-stiffening due to finite extensibility of the network strands, and ③ an elastomer with molecularly-strained network strands due to steric repulsion between densely grafted side chains, where n_x—the DP of the backbone in the bottlebrush strand, n_{sc}—the DP of the side chains, and n_g—the DP of the backbone spacer between neighboring side chains. c) Nominal electric field (voltage normalized by h_0) as a function of areal expansion for the corresponding model elastomers described in (b). The broad red line indicates the region of electric breakdown, which depends on multiple experimental factors including thickness, anisotropic dielectric permittivity, and device construction.[28] Dashed lines indicate continued electroactuation beyond the EMI.

examples of such actuators: i) a deflecting diaphragm and ii) an elongating tube. In the first case (Figure 2a), an as-cast PDMS bottlebrush elastomer film (n_{sc} = 14, n_g = 1, n_x = 200, and thickness h_0 = 0.44 mm) undergoes over 4× areal expansion prior to electrical breakdown (Movie S1, Supporting Information). In the second example (Figure 2b), a molded tube of identical elastomer (wall thickness h_0 = 0.80 mm and tube diameter D_0 =11 mm) displays reversible elongation and dilation at low voltages prior to uneven bulging at $\varepsilon_a^{EMI} \cong 59\%$ (Movie S2 and S3, Supporting Information). The diaphragm actuator has achieved a freestanding areal electroactuation ($\varepsilon_a \cong 300\%$) beyond those typically seen in prestrained silicone materials[1] and on par with commonly employed VHB acrylic actuators.[5] Furthermore, the actuating diaphragm can lift a ball 30× heavier than the actuator, displaying an excellent payload to mass ratio (Movie S4, Supporting Information). The tube sample also displays high and stable performance ($\varepsilon_a \cong 30\%$), comparable to so-called spring-roll actuators, achieving 25% stroke.[29] These results are particularly noteworthy as they were achieved for freestanding, as-cast shapes subjected to neither mechanical nor chemical modification unlike the current state-of-the-art materials.

Elimination of polymer chain entanglements in bottlebrush systems allows tuning bulk mechanical properties over a remarkably broad range without changing chemical composition. By independently varying the side-chain length, grafting density and crosslink density, we can synthesize DEs with Young's moduli ranging from 1 MPa down to ≈100 Pa and elongations at break up to ≈10.[30] In light of the unique properties achievable with bottlebrush elastomers, we first outline the basic principles of architectural control over mechanical properties. For a broad class of unentangled polymer networks, it has been demonstrated[31] that the stress–strain relation can be expressed in universal form as:

$$\sigma_{\text{true}}(\lambda) = \frac{G}{3}\left(\lambda^2 - \lambda^{-1}\right)\left[1 + 2\left(1 - \frac{\beta I_1(\lambda)}{3}\right)^{-2}\right] \quad (1)$$

where $I_1(\lambda) = \lambda^2 + 2/\lambda$ corresponds to the first invariant for uniaxial network deformation at a constant volume. Thus, the elasticity of a bottlebrush network is effectively described by two molecular parameters—i) the structural shear modulus ($G \cong \rho k_B T/n_s$) characterized by the number of monomeric units in the network strand $n_s \cong n_x(n_{sc}/n_g + 1)$, and ii) the strand elongation ratio at rest ($\beta = \langle R_{in}^2 \rangle / R_{max}^2$) defined as the ratio of the mean square end-to-end distance of a network strand in the as-prepared elastomer and the square of the length of a fully extended strand. Here, ρ—the monomer number density, k_B—the Boltzmann constant, and T—absolute temperature. It is important to recognize that β controls the strain-stiffening behavior required for stable electroactuation. Unlike linear-chain systems ($n_{sc} = 0$), for which G and β depend only on crosslink density as $\sim n_x^{-1}$,

Adv. Mater. 2016,
DOI: 10.1002/adma.201604209

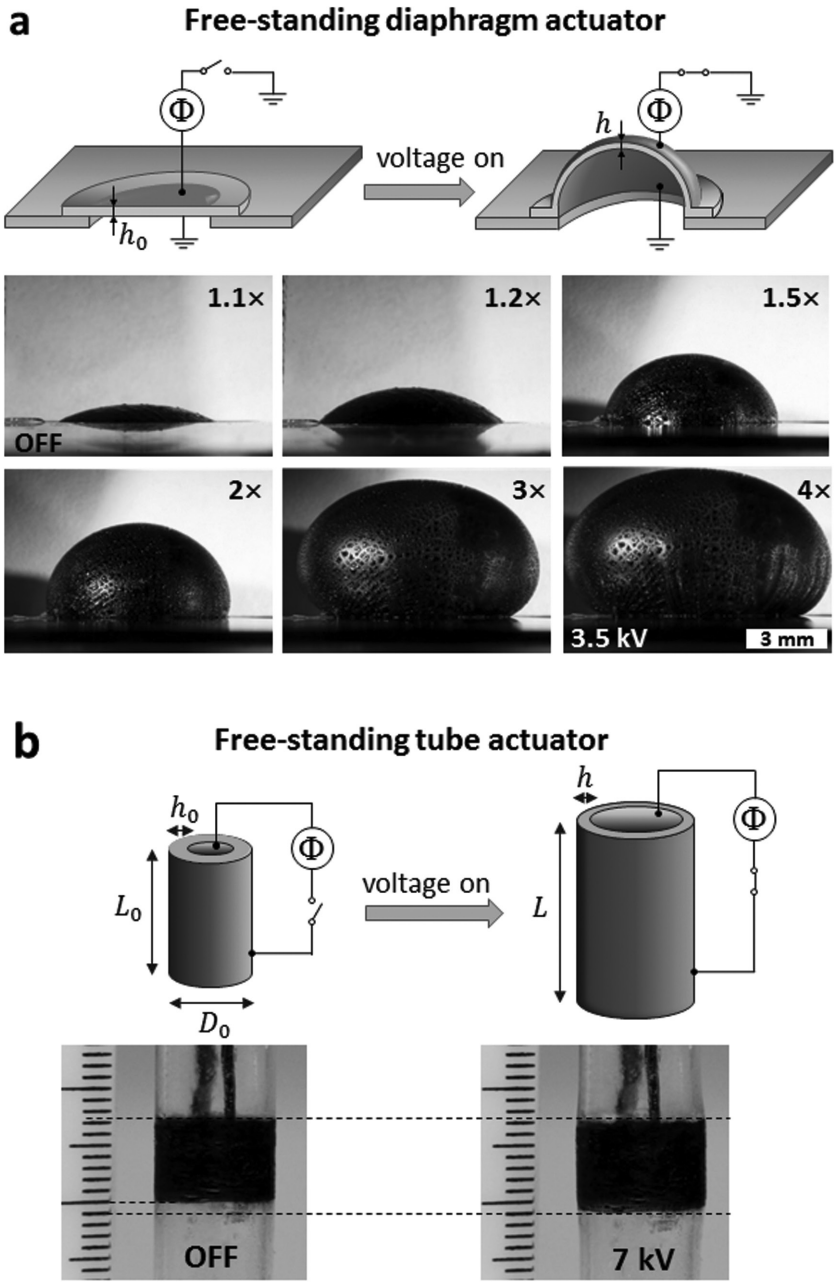

Figure 2. Freestanding DE actuators. a) Deflection of a circular diaphragm (h_0 = 0.44 mm) and b) uniaxial extension and lateral dilation of a tube (h_0 =0.80 mm and D_0 =11 mm) are evident upon electroactuation with increasing voltage Φ (Movie S1–4, Supporting Information). The numbers in (a) indicate field-induced areal expansion $\lambda_a = A/A_0 = h_0/h$ under isochoric conditions. The maximum strains achieved in the diaphragm and tube actuators were $\varepsilon_a = (\lambda_a - 1)\,100\% = 300 \pm 50\%$ and 25±5%, respectively. Both samples employ the same PDMS bottlebrush elastomer (Table 1: $n_{sc} = 14$, $n_g = 1$, $n_x = 200$). Larger tube elongations are possible as seen in Movie S3 in the Supporting Information, which shows electroactuation ($\varepsilon_a = 32 \pm 5\%$) of a softer tube ($n_x = 400$).

bottlebrush elastomers allow for orthogonal control of modulus and extensibility through variation of the backbone fraction n_g/n_{sc} as Equation (2) and (3):[30]

$$G = C_1 \frac{\rho k_B T}{n_x \left(n_{sc}/n_g + 1\right)} \sim \frac{n_g}{n_{sc}} n_x^{-1} \tag{2}$$

$$\beta = C_2 \left(\frac{n_{sc}}{n_g} + 1\right)^{1/2} n_x^{-1} \cong \sqrt{\frac{n_{sc}}{n_g}} n_x^{-1} \tag{3}$$

where C_1 and C_2 are numerical prefactors on the order of unity (0.3 and 3.1 obtained for our systems in **Figure 3**b) that account for specific network compositions. From Equation (2) and (3), we can draw several important conclusions relevant to the performance of DE actuators. First, bottlebrush networks are softer than their entangled linear-chain counterparts, which allows for larger actuator stroke at lower voltages. Second, the additional architecture parameter $\varphi = n_g/n_{sc}$ (molar fraction of the bottlebrush backbone) allows for simultaneous reduction of the modulus ($G \sim \varphi$) and enhancement of strain-stiffening ($\beta \sim \varphi^{-1/2}$), which provides an unexplored molecular-level approach for tuning DE elasticity. Third, independent synthetic control of n_x, n_{sc}, and n_g permits variation of DE mechanical properties over much broader and previously inaccessible ranges as demonstrated below.

Two series of bottlebrush elastomers with poly(dimethylsiloxane) (PDMS) side chains possessing n_{sc} = 14 and 28 have been prepared by photoinitiated radical polymerization of monofunctional macromonomers in the presence of difunctional crosslinkers (Figure S2, Supporting Information). All molecular characteristics are summarized in **Table 1**. Unlike previously reported synthetic strategies,[32] the method developed here allows one-step preparation of different macroscopic shapes at gel fractions of 91 ± 4%. Figure 3a displays stress–strain curves measured upon uniaxial extension of PDMS bottlebrush elastomers with n_{sc} = 14 (solid lines) and n_{sc} = 28 (long dashed lines). All curves display the characteristic strain-stiffening behavior due to finite extensibility of the intrinsically extended bottlebrush strands. As anticipated, the networks with smaller n_x and larger n_{sc} display more pronounced nonlinearity due to greater extension of the network strands ($\beta \sim \sqrt{n_{sc} n_x^{-1}}$). The stress–strain curves in Figure 3a are fitted using Equation (1) with the two parameters introduced earlier: G and β (short dashed lines in Figure 3a). Table 1 lists the regressed G and β values, as well as the apparent modulus (G_0) and elongation at break ($\lambda_{max,ex}$) measured at small and high strains, respectively. In Figure 3b, the values of G and β are plotted as a function of n_x^{-1} (an effective measure of crosslink density) and demonstrate excellent agreement with the scaling relationships provided by Equation (2) and (3). Such agreement highlights the consistency of both the bottlebrush architecture and the synthetic methods used to control it.

DOI: 10.1002/adma.201604209

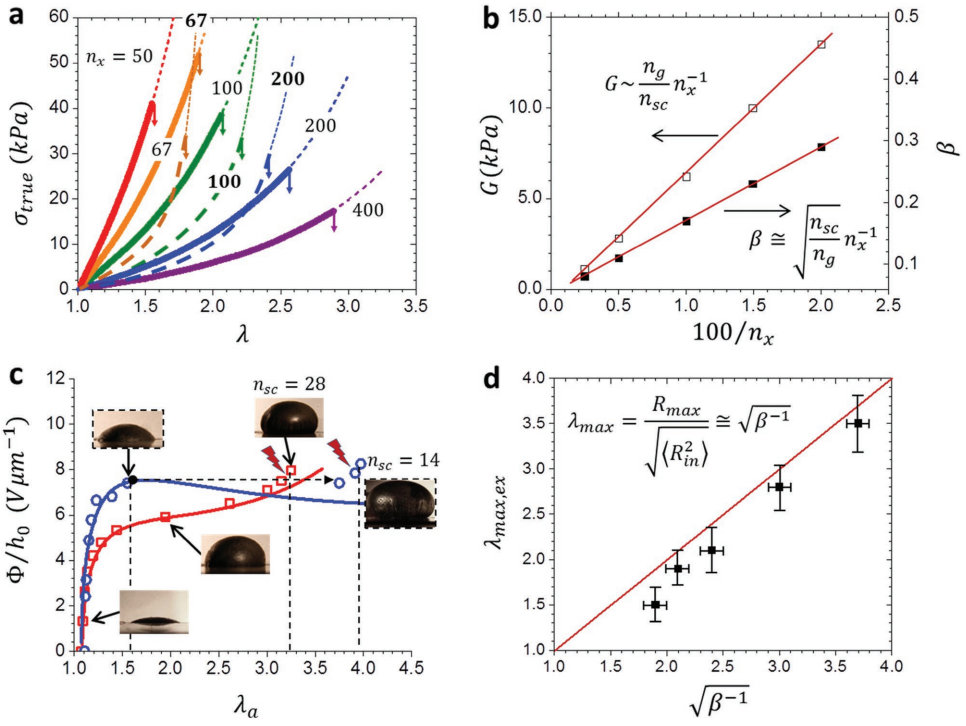

Figure 3. Electroactuation of bottlebrush elastomers. a) True stress is presented as a function of uniaxial extension upon tensile deformation of bottlebrush elastomers with different crosslink densities (n_x^{-1}) and side-chain DPs (n_{sc}). The color-matched solid and long dashed lines correspond to the sample series with $n_{sc} = 14$ and 28, (corresponding n_x values are indicated in plain and bold, respectively.) b) The shear modulus (G) and elongation ratio (β) extracted from fitting the stress–strain curves in (a) with Equation (1) (short dashed lines) are plotted as a function of n_x^{-1}. In accord with theoretical predictions, both properties increase linearly with increasing crosslink density. From the corresponding slopes and the known values of $n_{sc} = 14$, $n_g = 1$, and $\rho = 7.7$ nm^{-3} for PDMS, we obtain the numerical prefactors $C_1 = 0.3$ and $C_2 = 3.1$ in Equation (2) and (3). c) Electroactuation of two bottlebrush elastomers with the same network strand DP ($n_x = 200$) and two different side-chain DPs: 14 and 28. The experimental data points display favorable agreement with theoretical predictions (solid lines). The 10% offset in actuation is due to the biasing pressure $P = 5 \times 10^{-4}$ atm (Equation (4)). d) The experimental elongation at break ($\lambda_{max,ex}$) of the bottlebrush elastomers with $n_{sc} = 14$ is linearly dependent on the initial strand elongation $\sqrt{\beta^{-1}}$ (Equation (3)). Measurement error was calculated by taking the standard error of the mean from three measurements of uniaxial stress strain curves.

Taking a closer look at Figure 3a, it can be seen that all materials display relatively low moduli (1–10 kPa), relativley large extensions (up to 3.5), and enhanced strain stiffening response. These properties have direct implications for electroactuation, measured using the conventional diaphragm set-up pictured in Figure 2a and described in detail elsewhere.[5] Bottlebrush elastomers make use of weak electric fields to achieve large actuations, but with the price of relatively low tensile strength. This

Table 1. Structural parameters and mechanical properties of bottlebrush samples.

Sample	n_{sc} [a]	n_x [b]	$10^3\phi_x$ [c]	G [d] [kPa]	β [e]	G_0 [f] [kPa]	λ_{max} [g]	$\lambda_{max,ex}$ [h]
Series 1	14	400	1.2	1.1 ± 0.1	0.08 ± 0.01	1.2 ± 0.1	3.7 ± 0.2	3.5 ± 0.3
	14	200	2.5	2.8 ± 0.1	0.11 ± 0.01	3.3 ± 0.1	3.0 ± 0.2	2.9 ± 0.2
	14	100	5.0	6.2 ± 0.2	0.17 ± 0.01	8.1 ± 0.1	2.4 ± 0.1	2.1 ± 0.2
	14	67	7.4	10.0 ± 0.4	0.23 ± 0.01	15.0 ± 0.2	2.1 ± 0.1	1.9 ± 0.2
	14	50	9.9	13.5 ± 0.5	0.28 ± 0.02	22.0 ± 0.3	1.9 ± 0.1	1.5 ± 0.1
Series 2	28	200	2.5	1.1 ± 0.1	0.23 ± 0.01	1.5 ± 0.2	2.1 ± 0.1	2.4 ± 0.1
	28	100	5.0	1.8 ± 0.1	0.25 ± 0.02	2.7 ± 0.2	2.0 ± 0.1	2.2 ± 0.1
	28	67	7.4	2.0 ± 0.1	0.30 ± 0.02	3.4 ± 0.2	1.8 ± 0.1	1.9 ± 0.1

[a]Degree of polymerization (DP) of the side chain (Figure 1b); [b]Targeted DP of the backbone between crosslinks calculated from the mole fraction of the difunctional crosslinker as $n_x = 1/(2\varphi_x)$. Although the actual n_x values may be larger due to incomplete conversion of the crosslinker moieties, precise control of the crosslink density as linearly proportional to n_x^{-1} is accomplished (Figure 3b); [c]Mole fraction of crosslinker used in the synthesis; [d]Structural shear modulus; [e]Elongation of network strands in as-prepared bottlebrush elastomers determined by fitting the stress–strain curves in Figure 3a with Equation (1); [f]Apparent shear modulus measured as the slope $G_0 = d\sigma/d\lambda$ at small deformations ($\lambda \to 1$); [g]Maximum uniaxial extension calculated as $\sqrt{\beta^{-1}}$; [h]Experimentally measured elongation at break. All measurement error was calculated by taking the standard error of the mean from three measurements of uniaxial stress–strain curves.

Adv. Mater. **2016**,
DOI: 10.1002/adma.201604209

is in agreement with one of the "golden rules" for elastomeric materials, for which the engineering strength is inversely proportional to extensibility $\sigma_{max} \cong G\lambda_{max} \sim 1/\lambda_{max}$. As shown in Figure 3a, depending on the crosslink density, the mechanical stress required to achieve large deformations of bottlebrush elastomers may be two-three orders in magnitude lower than the stress in conventional elastomeric materials. This discourages the use of soft actuators for counteracting large sustained loads at low strain. However, these materials are perfectly suited for generating large actuations in low stress environments, using comparatively weak electric fields.

Figure 3c displays two characteristic examples of electroactuation for bottlebrush elastomers with and without EMI (see Figure S3 for more examples, Supporting Information). In the first case, a PDMS bottlebrush elastomer with a short side chain ($n_{sc} = 14$) and long strand ($n_x = 200$) exhibits EMI, which is evidenced by a drastic snap-through at a constant nominal electric field $\Phi/h_0 = 7.6\ \mathrm{V\,\mu m^{-1}}$. Note that the elastomer survives continued electroactuation from $\lambda_a^{EMI} \cong 1.6$ to $\lambda_a \cong 3.8$ and eventually undergoes dielectric breakdown at $\lambda_a^{BD} \cong 4.0$ and a true field of $33 \pm 5\ \mathrm{V\,\mu m^{-1}}$ (Figure S4, Supporting Information). Between $\lambda_a = 3.8$ and $\lambda_a^{BD} \cong 4.0$, electroactuation is stabilized by the finite extensibility of the network strands. The second example considered here (without EMI) corresponds to an elastomer with longer side chains ($n_{sc} = 28$) and exhibits steady voltage-controlled electroactuation over the entire extension range until dielectric breakdown occurs at $\lambda_a^{BD} \cong 3.2$. In both instances, the experimental data points are consistent with theoretical predictions (solid lines in Figure 3c and Equation (S4) in the Supporting Information) given as:

$$\frac{\Phi}{h_0} = (\varepsilon\varepsilon_0)^{-1/2}\sqrt{-\lambda^2\sigma_{true}(\lambda) - \frac{PR}{4h_0}\frac{1}{\sqrt{\lambda^{-1}-1}}} \quad (4)$$

where $\varepsilon_0 = 8.85 \times 10^{-12}\ \mathrm{F\,m^{-1}}$ is the dielectric permittivity of vacuum, $\varepsilon = 2.94 \pm 0.02$ refers to the relative dielectric permittivity of the elastomer (Figure S5, Supporting Information), $P = 5 \times 10^{-4}$ atm represents the blowing pressure to bias the actuation direction, and $R = 5$ mm is the radius of the DE membrane. In addition to governing the strain-stiffening behavior, the parameter β predicts the maximum extensibility of an ideal network as $\lambda_{max} \cong R_{max}/\sqrt{\langle R_{in}^2\rangle} \cong \sqrt{\beta^{-1}}$. As evidenced in Figure 3d and Table 1, the experimentally measured elongation at break ($\lambda_{max,ex}$) correlates reasonably well with the predicted λ_{max}. Note that, in our experiments (Figure 3a), the $\lambda_{max,ex}$ values, ranging from 1.9 to 3.5, mostly exceed the breakdown elongation $\lambda^{BD} \cong \sqrt{\lambda_a^{BD}} \cong 2$ (Figure 3c).

In summary, we have developed a bottom-up synthetic strategy of single-component DEs that enable moldable and freestanding electroactuators by incorporating bottlebrush strands in polymer networks. The effective actuation performance (normalized by mass of the total actuator assembly) of these materials are on par with skeletal muscle,[33] prestrained DEs, and commercial piezoelectric, hydraulic, and shape memory manipulators.[5,9,20,34,35] Specifically, bottlebrush DEs generate large strains > 300% and effective work densities ≈10 kJ m^{-3} at electromechanical efficiencies of ≈50% (Equation (S7), (S8), and (S9)) under relatively mild field conditions (<10 V μm^{-1}). The molecular design approach developed here is independent of chemistry and accesses a new range of freestanding actuation properties from materials with traditionally modest electroactuation performance (e.g., PDMS). The excellent baseline performance and myriad of chain-end functionalities afforded by the brush architecture open the use of bottlebrush elastomers as a highly versatile platform for the creation of novel copolymers and composites that undergo extreme changes in modulus, elasticity, and density, and ultrasoft moldable elastomers from physical networks for use in many soft-matter fields including medicine, robotics, and dielectric actuators.[16–18]

Experimental Section

Materials and Synthesis: Monomethacryloxypropyl-terminated poly(dimethylsiloxane) (MCR-M11, with an average molar mass of 1000 g mol^{-1}), monoaminopropyl-terminated poly(dimethylsiloxane) (MCR-A12 with an average molecular mass of 2000 g mol^{-1}) and α,ω-methacryloxypropyl-terminated poly(dimethylsiloxane) (DMS-R18 and DMS-R22) with different average molar masses (5000 and 10000 g mol^{-1}, respectively) were purchased from Gelest. All macromonomers were purified by passing through a basic alumina column to remove the inhibitor. Methacryloyl chloride (purity >97%), phenyl*bis*(2,4,6-trimethyl-benzoyl)phosphine oxide, triethylamine, copper chloride, *Tris*[2-(dimethylamino)ethyl]amine (Me_6TREN), ethyl 2-bromo-2-methyl propionate, dimethyl formaldehyde, tetrahydrofuran (THF), *p*-xylene were purchased from Aldrich and used as received. All other reagents and solvents were purchased from Aldrich and used without further purification.

Elastomer Film and Tube Preparation: All elastomers were prepared by a one-step polymerization of monomethacryloxypropyl-terminated poly(dimethylsiloxane) (MCR-M11, 1000 g mol^{-1}, M12 2000 g mol^{-1}) with different molar ratios of crosslinker (DMS-R18 and DMS-R22 for making elastomers with M11 and M12, respectively), as listed in Table 1 of the main text. The initial reaction mixture contained 57 wt% of the monomers (M11 or M12), 32 mg of phenylbis(2,4,6-trimethyl-benzoyl) phosphine oxide as photoinitiator, and 9 g of *p*-xylene as a solvent. The mixtures of monomer (M11 or M12), crosslinker, and photoinitiator in *p*-xylene were degassed by nitrogen bubbling for 30 min. For preparation of an elastomer film, the mixtures were injected between two glass plates with different PDMS spacers measuring 0.25, 0.5, 1.0, and 3 mm. The elastomer films were then polymerized at ambient temperature under N_2 using a UV crosslinking chamber with a 365 nm UV lamp for 12 h (0.1 mW cm^{-2}, 10 cm distance). Elastomer tubes were prepared by injection of the above mixtures between two concentric cylindrical molds with inner and outer diameters of 9.5 and 12.5 mm respectively. The cylinders were then allowed to polymerize at similar condition as explained for elastomer film preparation. Films and tubes swelled in chloroform in a glass petri dish. After each 8 h, the chloroform was replaced with fresh chloroform to remove unreacted monomers. Then, the samples were deswelled with ethanol and dried in an oven at 50 °C oven. The conversion of monomers to elastomer (gel fraction) was measured as 87-95 wt% from the ratio of the sample mass after washing to that before washing.

Characterization: The conversion of PDMS macromonomer during atom transfer radical polymerization was determined from ^{1}H NMR spectra recorded in deuterated chloroform ($CDCl_3$) using a Brüker 400 MHz spectrometer. To measure monomer conversion in elastomers, unreacted monomers were washed out by swelling the elastomers in chloroform and deswelling in THF three times, followed by drying at ambient temperature and fully drying at 50 °C. To investigate the basic mechanical properties of the bottlebrush samples, the elastomer sample films were punched into dumbbell samples with bridge dimensions of 12 mm × 2 mm × 1–2 mm. The samples were loaded into an RSA-G2 DMA (TA Instruments) and subjected to a constant Hencky strain rate of 0.003 strain per second until rupture occurred. All bottlebrush films

were subjected to triplicate testing to ensure accuracy of the data. The resulting stress strain curves were then analyzed with Equation (1) using Origin 2016 software. To investigate the disentangled nature (low modulus rubber plateau) and highly elastic behavior of the bottlebrush polymers, the frequency spectra of the dynamic moduli were measured in a window of 0.01–100 rad s^{-1} over a range of temperatures and strains using a TA Instruments ARES-G2 rheometer (see the Supporting Information for full details). The time–temperature superposition principle was used to construct a master curve of modulus versus frequency with a reference temperature of 298 K using the Williams–Landel–Ferry equation (Figure S1a, Supporting Information).

Atomic force microscopy (AFM) images were produced by spin-casting a 0.05 mg mL^{-1} PDMS bottlebrush solution onto a cleaved mica substrate at 2000 rpm for 1 min. Imaging of individual molecules was performed in PeakForce QNM mode using a multimode AFM instrument (Brüker) equipped with a NanoScope V controller. Silicon probes were used with a resonance frequency of 50–90 Hz and a spring constant of ≈0.4 N m. Dielectric measurements were conducted using a parallel-plate setup on an Agilent 4294A impedance analyzer with the Agilent 16451B sample holder. The maximum potential was 1.0 V and the frequency was varied between 40 Hz and 1 MHz. The specimens were supported with a 50 mm diameter stainless steel electrode on one side, and a 5 mm diameter guarded electrode on the other. By determining the impedance magnitude (Z) and phase angle (θ) at various frequencies (f) with the impedance analyzer, the measured capacitance $C_{meas} = \sin\theta/(|Z|2\pi f)$, which describes the capacitance of a parallel resistor-capacitor (RC) circuit, was obtained. The authors equated C_{meas} with the capacitance of a parallel-plate model $C_{model} = \varepsilon\,\varepsilon_0\pi D^2/(4h)$ and solved for ε, *where* ε is the dielectric permittivity, ε_0 is the dielectric permittivity of vacuum (=8.85 × 10^{-12} F/m), D is the smaller electrode diameter, and h is film thickness. The films were slightly compressed during the dielectric constant measurements to ensure good contact between the films and the electrode. The thicknesses of the films were taken to equal the distance between the electrodes as determined using a micrometer gauge. The experimental error in these measurements was primarily due to errors in film thickness determination and was estimated to be less than 10%. Electroactuation performance was studied using a diaphragm actuator setup under prestrain-free experimental conditions. The elastomer films were placed into an actuation frame between two flat facing acrylic rings with a 10 and 20 mm circular opening for the top and bottom ring, respectively. Two concentric circular carbon grease electrodes were painted onto opposite sides of the film and connected to an outside voltage source via copper tape. With the film trapped between the acrylic rings, this assembly was then screwed on top of a diaphragm chamber setup (Supporting Information). A bias air pressure of 5 × 10^{-4} to 5 × 10^{-3} atm (depending on the elastomer film thickness) was controlled by a pressure regulator and applied such that, when the DE films were actuated, they deformed out of plane to form a raised dome shape. The low bias pressure was not sufficient to prestrain samples before actuation. The active area of the DE films (where carbon grease electrodes contact) was flat and circular with a diameter of 10.0 mm (before actuation). A high-voltage power supply (from Gamma High Voltage Research Co.) was used to drive the actuators. During actuation, increases in voltage were measured with a voltmeter. Images and video of actuation were acquired using a camera (Canon T4i, 18–55 mm lens). The actuation strain was calculated from the new film area as determined using side-profile images of the domes and determining the dome geometry with ImageJ software. The reported strain values are averages of three measurements for each particular voltage. The nominal electric field was calculated by dividing the applied voltage by the initial thickness of the elastomer film. The breakdown field was calculated by dividing the applied voltage by the instantaneous thickness of the elastomer film at maximum strain.

Supporting Information

Supporting Information is available from the Wiley Online Library or from the author.

Acknowledgements

The authors gratefully acknowledge funding from the National Science Foundation (DMR 1122483, DMR 1407645, DMR 1436201, and DMR 1409710) and from Becton Dickinson Technologies. The authors also thank Dr. Edward Samulski for illuminating discussions and reviewing the manuscript.

Received: August 5, 2016
Revised: August 31, 2016
Published online:

[1] R. Pelrine, R. Kornbluh, Q. Pei, J. Joseph, *Science* **2000**, *287*, 836.
[2] F. Carpi, S. Bauer, D. De Rossi, *Science* **2010**, *330*, 1759.
[3] S. Kim, C. Laschi, B. Trimmer, *Trends Biotechnol.* **2013**, *31*, 287.
[4] D. Trivedi, C. D. Rahn, W. M. Kier, I. D. Walker, *Appl. Bionics Biomech.* **2008**, *5*, 99.
[5] P. Brochu, Q. Pei, *Macromol. Rapid Commun.* **2009**, *31*, 10.
[6] L. J. Romasanta, M. A. Lopez-Manchado, R. Verdejo, *Prog. Polym. Sci.* **2015**, *51*, 188.
[7] S. M. Ha, W. Yuan, Q. Pei, R. Pelrine, S. Stanford, *Adv. Mater.* **2006**, *18*, 887.
[8] D. M. Opris, M. Molberg, C. Walder, Y. S. Ko, B. Fischer, F. A. Nüesch, *Adv. Funct. Mater.* **2011**, *21*, 3531.
[9] J. D. Madden, *Science* **2007**, *318*, 1094.
[10] R. D. Kornbluh, R. Pelrine, Q. Pei, R. Heydt, S. Stanford, S. Oh, J. Eckerle, *Proc. SPIE Int. Soc. Opt. Eng.* **2002**, *4698*, 254.
[11] A. Cho, *Science* **2000**, *287*, 783.
[12] J. Biggs, K. Danielmeier, J. Hitzbleck, J. Krause, T. Kridl, S. Nowak, E. Orselli, X. Quan, D. Schapeler, W. Sutherland, J. Wagner, *Angew. Chem., Int. Ed.* **2013**, *52*, 9409.
[13] Y. Bar-Cohen, *Biomimetics: Biologically Inspired Technologies*, Taylor & Francis Group, Boca Raton, FL, USA **2005**.
[14] C. Keplinger, J. Y. Sun, C. C. Foo, P. Rothemund, G. M. Whitesides, Z. Suo, *Science* **2013**, *341*, 984.
[15] R. Shankar, T. K. Ghosh, R. J. Spontak, *Soft Matter* **2007**, *3*, 1116.
[16] C. H. Li, C. Wang, C. Keplinger, J. L. Zuo, L. Jin, Y. Sun, P. Zheng, Y. Cao, F. Lissel, C. Linder, X. Z. You, Z. Bao, *Nat. Chem.* **2016**, *8*, 618.
[17] C. Racles, M. Cazacu, B. Fischer, D. M. Opris, *Smart Mater. Struct.* **2013**, *22*, 104004.
[18] F. B. Madsen, L. Yu, A. E. Daugaard, S. Hvilsted, L. A. Skov, *Polymer* **2014**, *55*, 6212.
[19] S. Shian, R. M. Diebold, D. R. Clarke, *Opt. Express* **2013**, *21*, 8669.
[20] J. S. Plante, S. Dubowsky, *Int. J. Solids Struct.* **2006**, *43*, 7727.
[21] X. Zhao, Z. Suo, *Phys. Rev. Lett.* **2010**, *104*, 178302.
[22] P. H. Vargantwar, A. E. Özçam, T. K. Ghosh, R. J. Spontak, *Adv. Funct. Mater.* **2012**, *22*, 2100.
[23] X. Niu, H. Stoyanov, W. Hu, R. Leo, P. Brochu, Q. Pei, *J. Polym. Sci. B: Polym. Phys.* **2013**, *51*, 197.
[24] C. Keplinger, T. Li, R. Baumgartner, Z. Suo, S. Bauer, *Soft Matter* **2012**, *8*, 285.
[25] D. Rus, M. T. Tolley, *Nature* **2015**, *521*, 467.
[26] F. Carpi, G. Frediani, S. Turco, D. De Rossi, *Adv. Funct. Mater.* **2011**, *21*, 4152.
[27] F. Carpi, D. De Rossi, R. Kornbluh, R. E. Pelrine, P. Sommer-Larsen, *Dielectric Elastomers as Electromechanical Transducers*, Elsevier, Amsterdam, The Netherlands **2008**.
[28] A. Tröls, A. Kogler, R. Baumgartner, R. Kaltseis, C. Keplinger, R. Schwödiauer, I. Graz, S. Bauer, *Smart Mater. Struct.* **2013**, *22*, 104012.
[29] Q. Pei, M. Rosenthal, S. Stanford, H. Prahlad, R. Pelrine, *Smart Mater. Struct.* **2004**, *13*, N86.

DOI: 10.1002/adma.201604209

[30] W. F. M. Daniel, J. Burdyńska, M. Vatankhah-Varnoosfaderani, K. Matyjaszewski, J. Paturej, M. Rubinstein, A. V. Dobrynin, S. S. Sheiko, *Nat. Mater.* **2016**, *15*, 183.
[31] A. V. Dobrynin, J. M. Y. Carrillo, *Macromolecules* **2011**, *44*, 140.
[32] S. S. Sheiko, B. S. Sumerlin, K. Matyjaszewski, *Prog. Polym. Sci.* **2008**, *33*, 759.
[33] T. Mirfakhrai, J. D. Madden, R. H. Baughman, *Mater. Today* **2007**, *10*, 30.
[34] R. D. Kornbluh, R. Pelrine, H. Prahlad, A. Wong-Foy, B. McCoy, S. Kim, J. Eckerle, T. Low, *MRS Bull.* **2012**, *37*, 246.
[35] J. Peirs, D. Reynaerts, H. Van Brussel, *Proc. MME 2001 (Micromechanics European Workshop)* **2001**, p. 271.